INL/CON-23-71226-Revision-0

NOTCH EFFECT ON CREEP-FATIGUE BEHAVIOR OF ALLOY 617 AT ELEVATED TEMPERATURE

July 2023

Peijun Hou, Yanli Wang, Ting-Leung Sham

Changing the World's Energy Future

Idaho National Laboratory

INL is a U.S. Department of Energy National Laboratory operated by Battelle Energy Alliance, LLC

INL/CON-23-71226-Revision-0

NOTCH EFFECT ON CREEP-FATIGUE BEHAVIOR OF ALLOY 617 AT ELEVATED TEMPERATURE

Peijun Hou, Yanli Wang, Ting-Leung Sham

July 2023

Idaho National Laboratory
Idaho Falls, Idaho 83415

http://www.inl.gov

Prepared for the
U.S. Department of Energy
Under DOE Idaho Operations Office
Contract DE-AC07-05ID14517

Proceedings of the ASME 2023
Pressure Vessels & Piping Conference
PVP2023
July 16-21, 2023, Atlanta, Georgia, USA

PVP2023-106503

NOTCH EFFECT ON CREEP-FATIGUE BEHAVIOR OF ALLOY 617 AT ELEVATED TEMPERATURE

Peijun Hou[1], Yanli Wang[2], Ting-Leung Sham[3]

[1]Imtech Corporation, Knoxville, Tennessee, USA
[2]Oak Ridge National Laboratory, Oak Ridge, Tennessee, USA
[3]Idaho National Laboratory, Idaho Falls, Idaho, USA

ABSTRACT

High-temperature reactor structural components are often under the complex multiaxial creep-fatigue (CF) loading conditions throughout the lifetime because of geometric and/or metallurgical discontinuities and complex loading paths. To assess the multiaxial CF deformation behavior and to evaluate the CF design rules in the ASME BPVC Section III, Division 5, Subsection HB, Subpart B, experimental and numerical studies are performed on Alloy 617 at 950°C using notch specimen geometries under CF loading in this study.

Two types of notch specimen geometries, shallow-notch and sharp V-notch were designed for Alloy 617 per ASTM Standard E292-09. Experimental procedures were developed, and tests at 950°C were performed under CF loading using the two notch specimen geometries. The information collected from the experiments included the average axial stress relaxation histories, the changes in the relaxation behavior as a function of applied cycles, and failure. Additionally, an inelastic constitutive model of Alloy 617 was used in the finite element analyses of the notch specimens to determine the stress triaxiality distributions, local and average stress relaxation behavior, and local elastic follow-up. The results from the experimental and numerical studies on the CF of notch specimens are compared with those on standard uniaxial smooth bar specimens. The notch effect on the CF deformation and failure of Alloy 617 are summarized and the assessment of the design rules regarding the treatment of multiaxial stress relaxation are discussed.

Keywords: Alloy 617; Notch; Multiaxial Creep-fatigue; Elastic follow-up; Stress triaxiality; High temperature

1. INTRODUCTION

The material degradation in the structural components under cyclic loading at elevated temperature is significantly influenced by the time-dependent creep-fatigue (CF) interaction. In the past several decades, researchers have devoted to the elevated temperature code rule development in the American Society of Mechanical Engineers (ASME) Boiler and Pressure Vessel Code (BPVC), Section III, Division 5 to ascertain conservative structural designs against CF failure for fast reactors. In general, advances in the CF performance of structural material are considered to be essential to realize the enhancement in the economics of very high temperature fast reactors.

In practice, the structural components are mostly under the multi-axial CF loading condition throughout the lifetime because of the geometric discontinuities and complicated loading path. However, the lab-scale CF testing data are generally collected from the standard uniaxial CF test and/or the simplified model test (SMT) uniaxial CF test, in which the time-dependent allowable stresses for ASME design purpose are determined by using the uniform dog-bone specimen [1-3]. Therefore, an experimental and accurate description of the multi-axial stress state and its influence on the stress relaxation behavior and CF life at critical locations of high-temperature component, in an attempt to develop the current structural designs, is necessary to be addressed. Furthermore, elastic follow-up caused by a mixed controlled loading mode (i.e., an intermediate loading mode between the stress-controlled and the strain-controlled modes) plays significant role in the time-dependent CF damage evolution. To investigate the multi-axial loading effect, the elastic follow-up effect is also needed to be taken into account.

To this end, we are aiming to collect multiaxial CF failure data and to demonstrate the effect of multi-axial stress state combined with elastic follow-up on the stress relaxation behavior and the reduction in the CF life. In this study, the nickel-

based Alloy 617 (UNS N06617) is focused, and this high-temperature structural material has been approved for elevated temperature service construction of Class A components conforming to the requirements of the ASME Section III, Division 5, Subsection HB, Subpart B "Elevated Temperature Service", for service temperature up to 1,750°F (954°C) and service life up to 100,000 hr, via Code Case N-898.

In this paper, standard tensile-hold CF tests were designed and carried out on notch specimens of Alloy 617 at 950°C. Two types of notch geometry (i.e, shallow-notch and sharp V-notch) was applied. The effect of notch geometries was studied in comparison to the standard CF testing data on the uniform specimens. In addition, a unified viscoplastic constitutive model was applied and conducted using finite element (FE) method with the purpose of estimating the distributions of the stress triaxiality factor and elastic follow-up factor and investigating their influences in stress relaxation behavior.

2. CREEP-FATIGUE EXPERIMENTS ON NOTCH SPECIMENS

The notch specimens were machined from an annealed Alloy 617 plate with Heat 314626 provided by ThyssenKrupp VDM. Table 1 presents the chemical composition of this alloy plate. The specimen longitudinal direction is oriented along the rolling direction of the material plate. All the specimens are tested in the as-received, solution-annealed condition.

Table 1. The chemical composition in wt.% of Alloy 617 plate with Heat 314626

Ni		S	Cr	C	Mn	Si
54.1		<0.002	22.2	0.05	0.1	0.1
Mo	**Ti**	**Cu**	**Fe**	**Al**	**Co**	**B**
8.6	0.4	0.04	1.6	1.1	11.6	<0.001

The notch specimen geometries used in this study for experimental CF tests are shown in Figure 1. Two types of specimens (i.e., shallow-notch and sharp V-notch) were designed. To simplify the specimen machining procedure and, the notches were machined on a straight bar of total length 7.0 in. (177.8 mm) at the mid-length location. The 0.75 in. (19.0 mm) straight-gauge at the center of specimen was mechanically polished. The straight bar section of the specimen has a diameter of 0.5 in. (6.35 mm) and the two types of notch design follows the ASTM Standard E292-09. The ratio of the outer diameter to inner diameter in both shallow-notch and V-notch specimens is approximately $\sqrt{2}$, which is recommended by the Code of Practice [4].

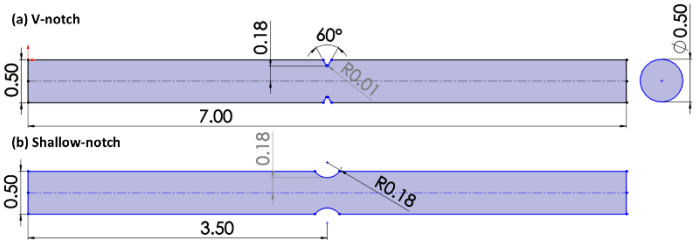

FIGURE 1: DIMENSIONS OF NOTCH SPECIMEN USED IN THE CF TESTS AT 950°C. (a) V-NOTCH AND (b) SHALLOW-NOTCH SPECIMENS. UNIT: IN.

It should be noted that the applied strain in CF tests for notch specimens is globally controlled in the section of nominal gauge length of the extensometer, as illustrated in Figure 2. Extensometer with a nominal gauge length of 0.5 in. (12.7 mm) was used to control the nominal axial strain in the gauge section. The standard CF testing procedure followed ASTM E2714-13 standard [5] under strain-controlled mode. The strain loading profile is shown schematically in Figure 3. The hold-time period is applied to the maximum tensile strain amplitude. The strain profile is fully reversed. The nominal strain rate is 1×10−3/s. Table 2 summaries the conditions of CF testing for notch specimens conducted at Oak Ridge National Laboratory (ORNL).

In this study, all tensile-hold standard CF experimental results of uniform specimens used for comparison to notch specimens were collected at Idaho National Laboratory (INL) [6].

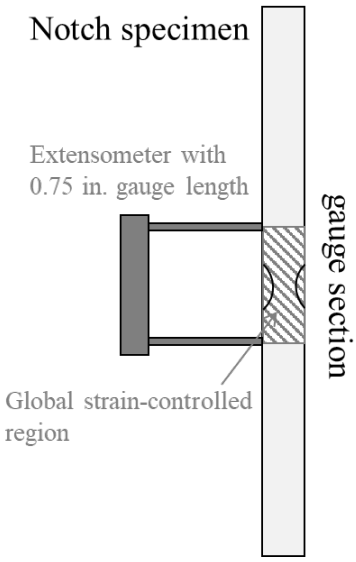

FIGURE 2: SCHEMATIC OF THE EXPERIMENTAL CF TEST SETUP FOR NOTCH SPECIMEN.

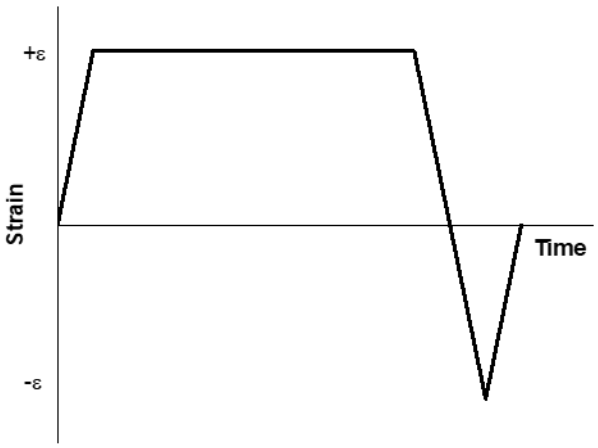

FIGURE 3: STRAIN-CONTROLLED CREEP-FATIGUE (CF) LOADING PROFILE FOR ONE CYCLE.

Table 2. Tensile-hold creep-fatigue test conditions on notch specimens for Alloy 617 at 950°C

Notch specimen	Nominal strain range, %	Strain rate, /s	Hold time, s
Shallow-notch	0.6	0.001	600
Shallow-notch	0.6	0.001	3600
V-notch	0.6	0.001	600
V-notch	0.6	0.001	3600

3. VISCOPLASTICITY FINITE ELEMENT MODELING

An axisymmetric FE simulation was conducted to calculate the stress field, strain field, and strain energy filed of notch specimens and to investigate the influences of stress triaxiality and elastic follow-up on stress relaxation behavior using the commercial software ABAQUS Standard. The numerical FE simulation used the same experimental CF conditions described in Section 2. In addition, 0.5 in. (12.7 mm) length of the gauge section for each notch specimen were only simulated in the FE model with the purpose of comparison to experimental data as the extensometers used in the experimental CF tests. It should be noted that specimens in the FE model were subjected to a global strain-controlling loading waveform with a total strain range of 0.6%, in Figure 3. The boundary conditions of uniform and notch specimens used in FE model is that the bottom surfaces were fixed in the loading direction (i.e., $u_y = 0$). The element type used is a four-node bilinear brick element (CAX4 in ABAQUS), and the lateral length of each element near notch root and notch boundaries is approximately 0.1 mm.

The finite element implementation is performed using the user-defined material (UMAT) subroutine in ABAQUS. This numerical modeling work is based on a unified viscoplasticity theory, which is briefly outlined below [7, 8].

This material model is governed by a time integration of the strain rate decomposition, that is given by:

$$\dot{\boldsymbol{\epsilon}} = \dot{\boldsymbol{\epsilon}}_{\boldsymbol{e}} + \dot{\boldsymbol{\epsilon}}_{\boldsymbol{in}} + \dot{\boldsymbol{\epsilon}}_{\boldsymbol{th}} \tag{5}$$

The elastic strain rate, $\dot{\boldsymbol{\epsilon}}_{\boldsymbol{e}}$, and the thermal strain rate, $\dot{\boldsymbol{\epsilon}}_{\boldsymbol{th}}$, are expressed as:

$$\dot{\boldsymbol{\epsilon}}_{\boldsymbol{e}} = \mathbf{C}^{-1}\!:\dot{\boldsymbol{\sigma}} \tag{6}$$

$$\dot{\boldsymbol{\epsilon}}_{\boldsymbol{th}} = \alpha\dot{T}\mathbf{I} \tag{7}$$

where $\dot{\boldsymbol{\epsilon}}_{\boldsymbol{in}}$ is the inelastic strain rate tensor, $\dot{\boldsymbol{\sigma}}$ is the stress rate tensor, $\mathbf{C}$ is the isotropic elasticity tensor calculated using the temperature-dependent elastic modulus and Poisson's ratio, α is the thermal expansion coefficient, and $\mathbf{I}$ is the identity tensor.

The inelastic strain rate is given by:

$$\dot{\boldsymbol{\epsilon}}_{\boldsymbol{in}} = \dot{\gamma}\frac{\partial f}{\partial \boldsymbol{\sigma}} \tag{8}$$

where $\dot{\gamma}$ is the consistency parameter, and f is the yield function, which is given by:

$$f = \sqrt{\frac{3}{2}(\mathbf{s}-\mathbf{x})\!:(\mathbf{s}-\mathbf{x})} - \sqrt{\frac{2}{3}(\sigma_0+\sigma_R)} \tag{9}$$

where $\mathbf{s}$ is the deviatoric stress tensor, $\mathbf{x}$ is the back stress tensor, σ_0 is the rate-independent threshold stress, and σ_R is the isotropic hardening deformation resistance. The back stress, $\mathbf{x}$, the threshold stress, σ_0, and the isotropic hardening deformation resistant, σ_R, are expressed as:

$$\mathbf{x} = \sum_i^3 \mathbf{x}_i \tag{10}$$

$$\dot{\mathbf{x}}_i = \left(\frac{2}{3}C_i\frac{\partial f}{\partial \boldsymbol{\sigma}} - \sqrt{\frac{2}{3}}\gamma_i\mathbf{x}_i\right)\dot{\gamma} \tag{11}$$

$$\dot{\sigma}_R = \delta(Q-\sigma_R)\dot{\gamma} \tag{12}$$

$$\sigma_0 = \mu e^{C_{km}} \tag{13}$$

where $\mathbf{x}_i$ is the back stress component tensor, $\dot{\mathbf{x}}_i$ is the back stress component rate tensor, C_i is the back stress component hardening rate, γ_i is the back stress component dynamic recovery rate, $\dot{\sigma}_R$ is the isotropic hardening rate, δ and Q are the temperature-dependent isotropic hardening parameters.

This viscoplsticity model is established to include rate-independent and rate-dependent deformation response based on the Kocks-Mecking (KM) diagram. The model for material rate sensitivity switches from a rate sensitive response to an insensitive response as the temperature and/or strain rate changes. In this model, the inelastic strain rate switches between a rate-dependent and a rate-independent response based on the Kocks-Mecking normalized activation energy, g, give as:

$$g = \frac{k(T + 273.15)}{\mu b^3} \log \frac{\dot{\epsilon}_0}{\sqrt{\frac{2}{3}\epsilon_{ij}\epsilon_{ij}}} \quad (14)$$

where k is the Boltzmann constant, μ is the shear modulus, b is the Burgers vector, and $\dot{\epsilon}_0$ is a reference strain rate. g_0 is defined as the critical normalized activation energy which identifies the rate-dependent regime and the rate-independent regime. When $g \leq g_0$, the model is rate-independent, and consistency parameter is given by those conditions:

$$\dot{\gamma} \geq 0 \quad (15)$$

$$f(\boldsymbol{\sigma}) \leq 0 \quad (16)$$

$$\dot{\gamma} f(\boldsymbol{\sigma}) = 0 \quad (17)$$

$$\dot{\gamma} \dot{f}(\boldsymbol{\sigma}) = 0 \quad (18)$$

When $g > g_0$, the model is rate-dependent, and the consistency parameter is given by the power-law viscoplastic theory defined as:

$$\dot{\gamma} = \sqrt{\frac{3}{2}} \langle \frac{f(\boldsymbol{\sigma})}{\sqrt{\frac{2}{3}}\eta} \rangle^n \quad (19)$$

$$\sigma_0 = 0 \quad (20)$$

$$n = \frac{-\mu b^3}{k(T + 273.15)A_{km}} \quad (21)$$

$$\eta = \frac{\mu e^{B_{km}}}{\dot{\epsilon}_0^{\,1/n}} \quad (22)$$

where A_{km} is the Kocks-Mecking slope, B_{km} is the Kocks-Mecking intercept, and C_{km} is the Kocks-Mecking horizontal asymptote, and $\langle ... \rangle$ denotes the Macaulay brackets.

All material parameters used in this study are from the Ref. [4] and are listed in Table 3. It should be noted that the parameters used in this model are for the case of the temperature of 950°C, although this material model can be adopted at different temperatures.

Table 3. Material parameters used in the unified viscoplastic constitutive model. [4]

Parameter	Value	Unit
Elastic modulus, E	136000	MPa
Poisson's ratio, υ	0.31	-
Boltzmann constant, k	1.38064×10^{-20}	mJ//°C
Burgers vector, b	2.747×10^{-7}	mm
Reference strain rate, $\dot{\epsilon}_0$	1.0×10^{10}	/s
KM slope, A_{km}	-7.985	-
KM intercept, B_{km}	-0.6696	-
KM horizontal asymptote, C_{km}	-5.550	-
KM intersection point, g_0	0.6112	-
Back stress 1 hardening rate, C_1	643.9330	Mpa
Back stress 2 hardening rate, C_2	40.3267	Mpa
Back stress 3 hardening rate, C_3	-20.6000	Mpa
Dynamic recovery rate 1, γ_1	103.700	-
Dynamic recovery rate 2, γ_2	5.089	-
Dynamic recovery rate 3, γ_3	0.9823	-
Isotropic strain hardening parameter, Q	-17.73	-
Isotropic strain hardening parameter, δ	10.32	-

4. RESULTS AND DISCUSSION

4.1 Experimental Results of Notch Specimens

The experimental results for notch specimens and uniform specimens used for comparison are summarized in Table 3. Comparing the experimental results between notch specimens and uniform specimens, the notch effect on reducing the CF life at the strain range, hold time, and temperature studied is indicated. Comparison of CF life of each notch specimen between 600 s and 3600 s tensile hold time shows that the effect of tensile hold time on the change in CF life of notch specimens is insignificant.

Table 3. Tensile-hold creep-fatigue test results on notch specimens for Alloy 617 at 950°C

Specimen	Nominal strain range, %	Hold time, s	Cycle to failure
Shallow-notch	0.6	600	295
Shallow-notch	0.6	3600	270
V-notch	0.6	600	-
V-notch	0.6	3600	-
Uniform A-14	0.6	600	550
Uniform B-18	0.6	600	700
Uniform B-19	0.6	600	600

Figure 4 presents the evolutions of the maximum, the minimum stresses, and the relaxation stresses of notch specimens and uniform specimens tested at strain range of 0.6% with 600 s tensile hold time. The comparison of the maximum and minimum stresses for notch and uniform specimens, Figure 4a, shows higher stresses in notch specimens. The V-notch specimen exhibits higher maximum stresses at initial cycles as compared to shallow-notch specimen, while V-notch specimen shows a continuous decrease in the maximum stresses as applied cycle increases in comparison to the nearly constant maximum stresses in shallow-notch specimen before the beginning of failure. In Figure 4b, notch specimens generally exhibit higher relaxation stresses at the end of the tensile hold of 600 s than uniform specimens. The difference in the relaxation stresses between V-notch and shallow-notch specimens is not significant. Figure 5 shows the comparison of stress-strain hysteresis loop and stress relaxation curve of the cycle 10 between notch and uniform specimens. In addition, the stress-relaxation curves in the notch specimens are normalized by initial stress during hold time stage and the results are presented in Figure 5c along with the normalized stress relaxation curve from the uniform specimens. In this comparison, both notch specimens show higher stresses

during the relaxation, and the relaxation stresses during hold are comparable between V-notch and shallow-notch specimens. However, the normalized relaxation stresses stay almost same among uniform and notch specimens, Figure 5c.

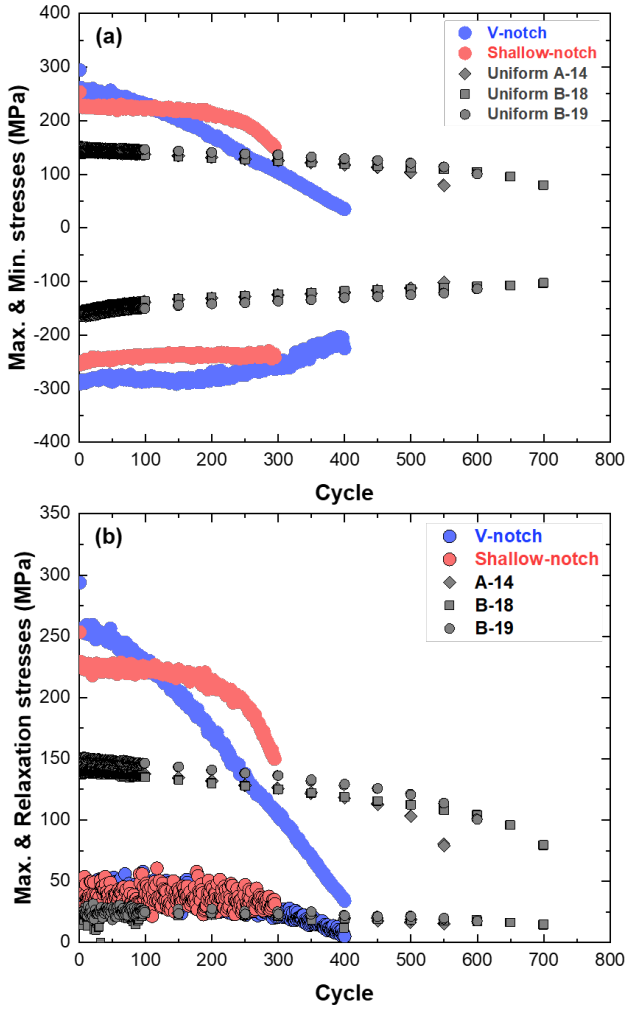

FIGURE 4: THE MAXIMUM, THE MINIMUM STRESSES, AND THE RELAXATION STRESSES OF NOTCH SPECIMENS AND UNIFORM SPECIMENS TESTED AT STRAIN RANGE OF 0.6% WITH 600 S TENSILE HOLD TIME.

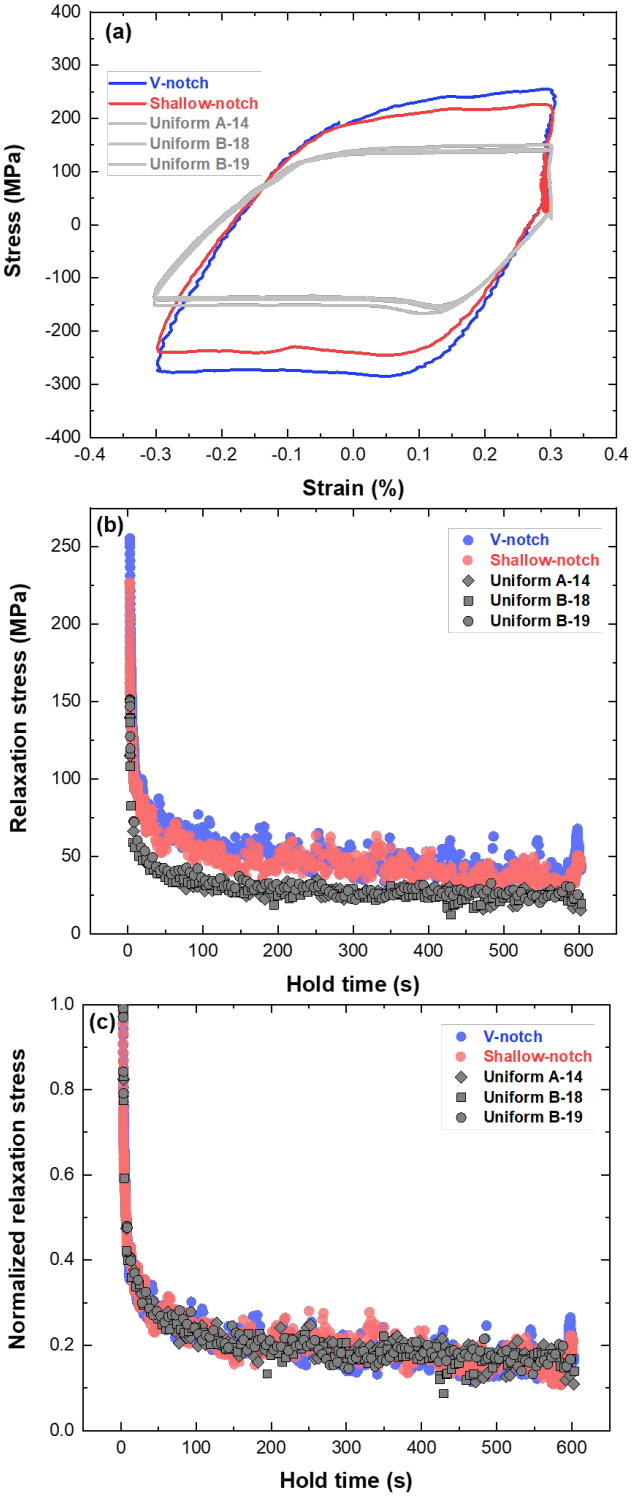

FIGURE 5: THE COMPARISON OF STRESS-STRAIN HYSTERESIS LOOP, STRESS RELAXATION CURVE, AND NORMALIZED STRESS RELAXATION CURVE OF THE CYCLE 10 BETWEEN NOTCH AND UNIFORM SPECIMENS.

Figure 6 shows the comparison of the maximum and minimum, and the relaxation stresses of V-notch specimen between 600 s and 3600 s tensile hold time. The maximum and minimum stresses in V-notch specimen with the hold time of 3600 s are quite similar to that of 600 s at initial cycles, while they become lower in the case of 3600 s as applied cycle increases. The V-notch specimen with 3600 s hold, in Figure 6b, is expected to show lower relaxation stresses at the end of the hold due to the longer hold time. Figure 7 shows the comparison of stress-strain hysteresis loop and stress relaxation curve of the cycle 10 in V-notch specimens with 600 s and 3600 s hold. This comparison shows that there is insignificant difference in stress-strain curve and relaxation curve. Similarly, comparisons of the maximum, the minimum, the relaxation stresses, the stress-strain hysteresis loop of the 10th cycle, and the stress relaxation curve of the 10th cycle of shallow-notch specimens between 600 s and 3600 s tensile hold time are presented in Figure 8 and Figure 9. The observations in the comparison of shallow-notch specimen in Figure 8 and Figure 9 are similar to that of V-notch specimen.

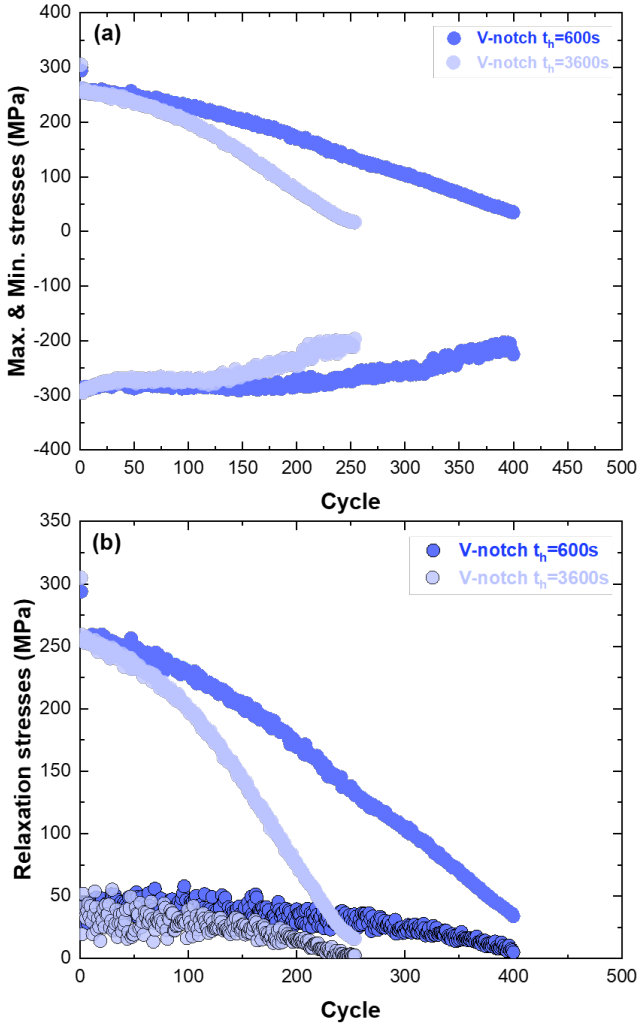

FIGURE 6: THE COMPARISON OF THE MAXIMUM AND MINIMUM, AND THE RELAXATION STRESSES OF V-NOTCH SPECIMEN BETWEEN 600 S AND 3600 S TENSILE HOLD TIME.

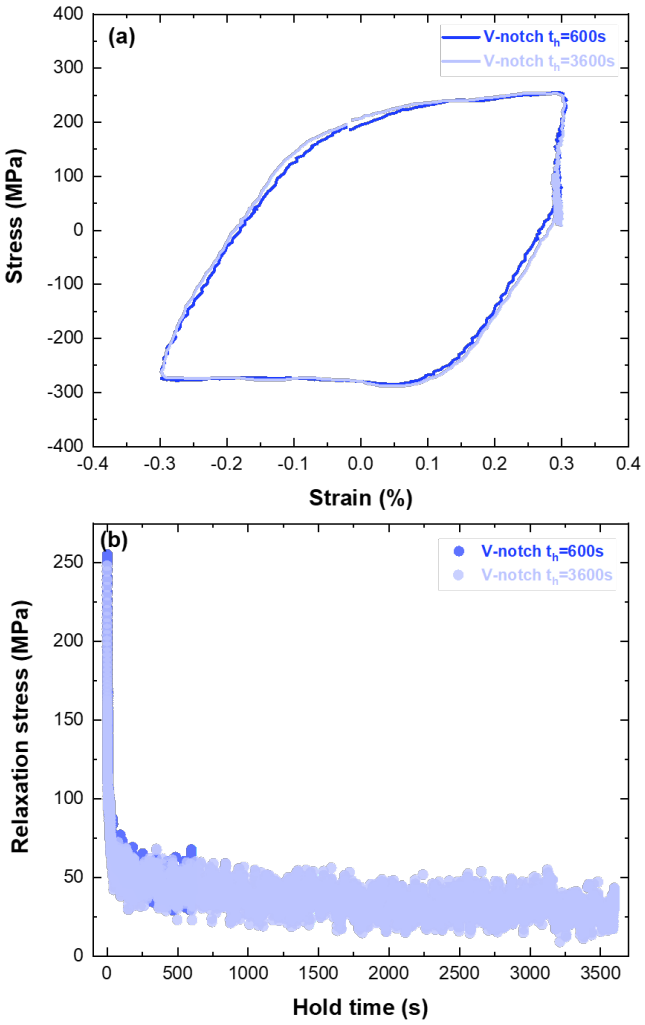

FIGURE 7: THE COMPARISON OF STRESS-STRAIN HYSTERESIS LOOP AND STRESS RELAXATION CURVE OF THE CYCLE 10 IN V-NOTCH SPECIMENS WITH 600 S AND 3600 S HOLD.

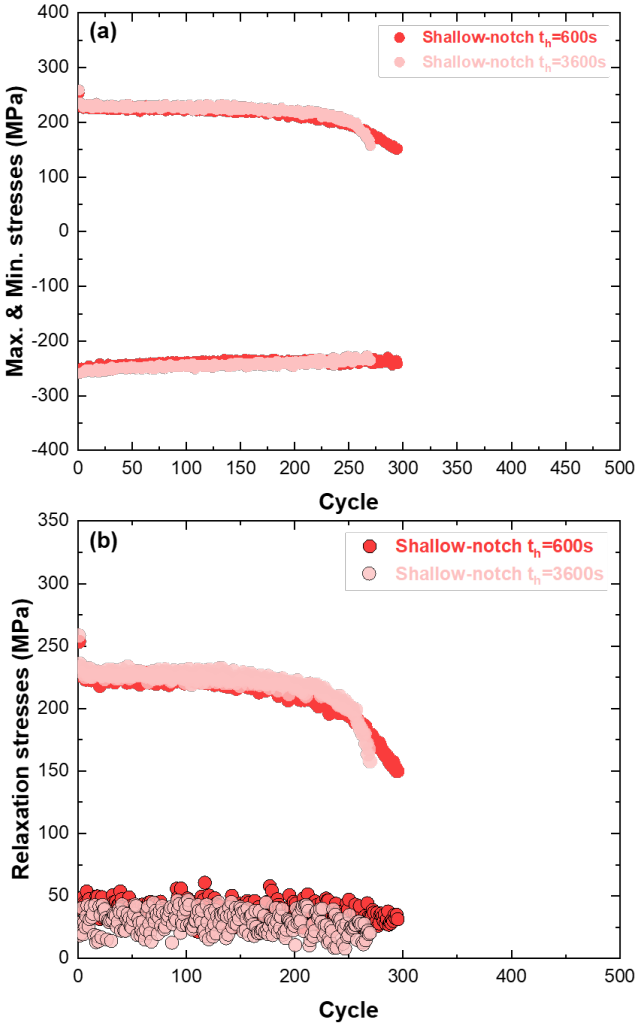

FIGURE 8: THE COMPARISON OF THE MAXIMUM AND MINIMUM, AND THE RELAXATION STRESSES OF SHALLOW-NOTCH SPECIMEN BETWEEN 600 S AND 3600 S TENSILE HOLD TIME.

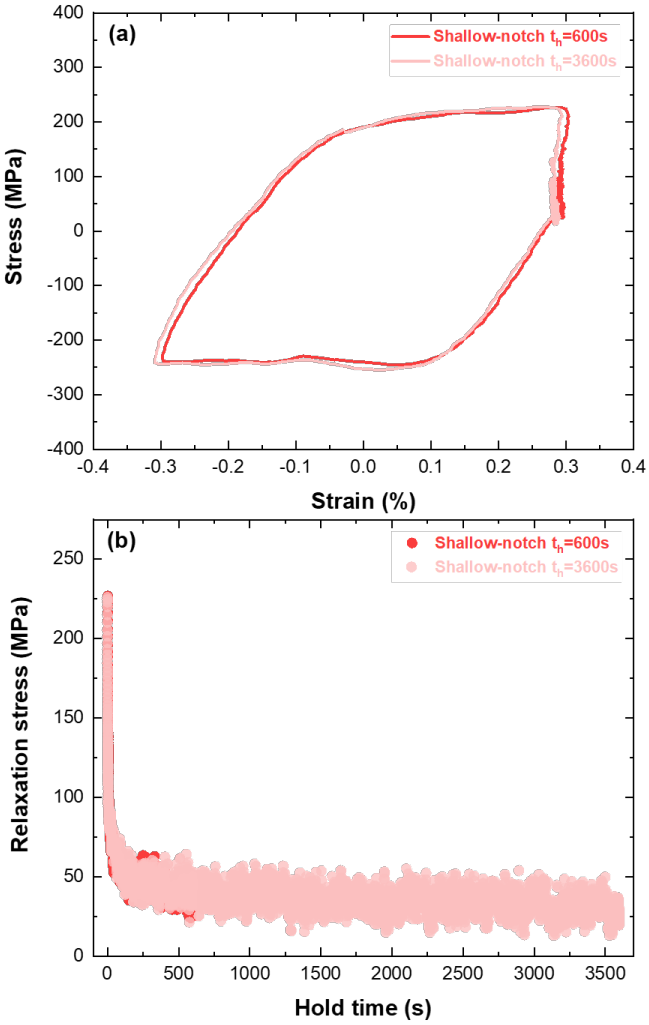

FIGURE 9: THE COMPARISON OF STRESS-STRAIN HYSTERESIS LOOP AND STRESS RELAXATION CURVE OF THE CYCLE 10 IN SHALLOW-NOTCH SPECIMENS WITH 600 S AND 3600 S HOLD.

4.2 Numerical Results of Notch Specimens

Figure 10 compares the stress relaxation curves at the 3rd cycle. A good agreement between experimental results, in Figure 5, and the numerical results, in Figure 10, has been achieved. Notch specimens show comparable stress relaxation rate to the uniform specimens.

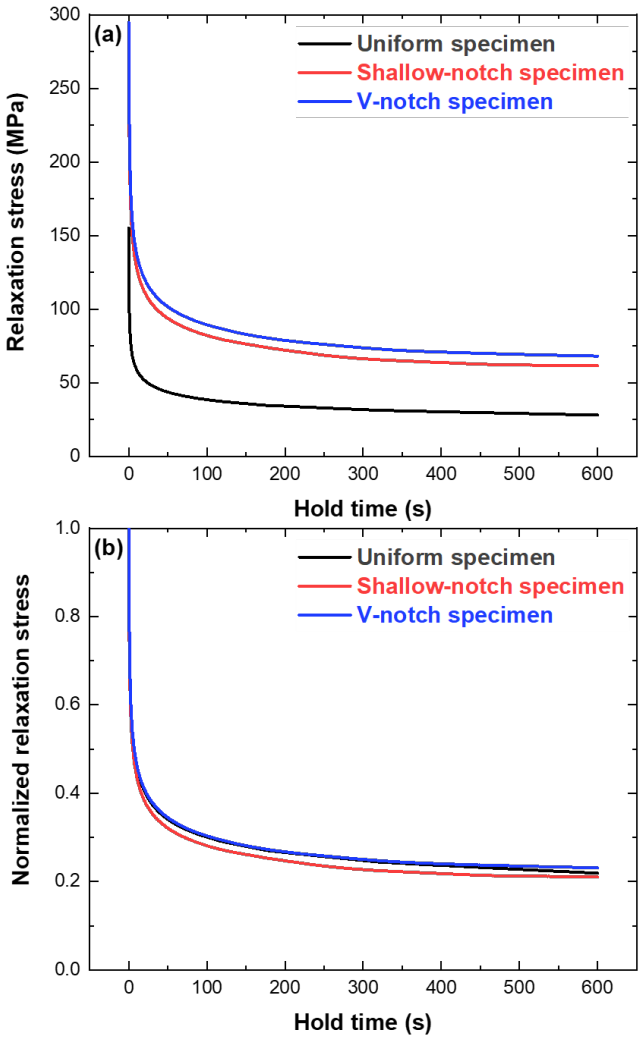

FIGURE 10: THE COMPARISON OF STRESS RELAXATION CURVE AND NORMALIZED STRESS RELAXATION CURVE OF THE CYCLE 3 BETWEEN NOTCH AND UNIFORM SPECIMENS.

To investigate the multiaxial stress effect, the stress triaxiality factor, TF, contours of the 3rd cycle are calculated according to Eq. 23 and are presented at the loading right before the holding and at the end of the holding period in Figure 11. The maximum stress TFs of the V-notch specimen and shallow-notch specimen are about 1.5 and 1.0, respectively.

$$TF = \frac{\frac{1}{3}\sigma_{ii}}{\sqrt{\frac{3}{2}S_{ij}S_{ij}}} \tag{23}$$

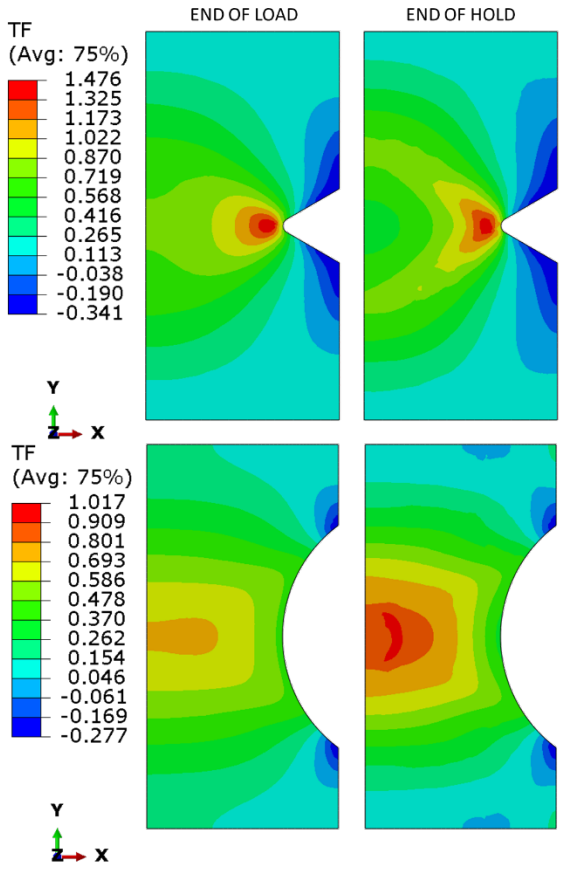

FIGURE 11: THE STRESS TRIAXIALITY FACTOR, TF, CONTOURS OF THE 3RD CYCLE AT THE LOADING RIGHT BEFORE THE HOLDING AND AT THE END OF THE HOLDING PERIOD.

Figure 12 shows the contours of the equivalent strain range of uniform and notch specimens. The maximum equivalent strain range of the V-notch specimen and shallow-notch specimen are 5.5% and 1.4%, respectively. The equivalent strain range will be used to incorporate to the experimental cycle to failure for the analysis and development of CF design curves.

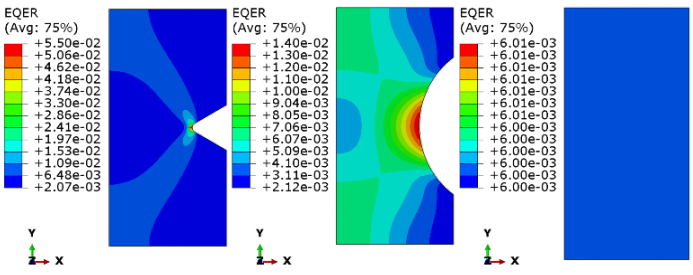

FIGURE 12: EQUIVALENT STRAIN RANGE CONTOUR OF UNIFORM AND NOTCH SPECIMENS

In addition, the contours of the inelastic strain rate at the initial 10 s hold of the 3rd cycle of uniform and notch specimens are presented in Figure 13. This numerical results illustrated the

effect of notch on changes in creep/inelastic deformation. V-notch and shallow-notch specimens show comparable inelastic strain rate, while it is 2 to 3 times higher than the value of uniform specimen.

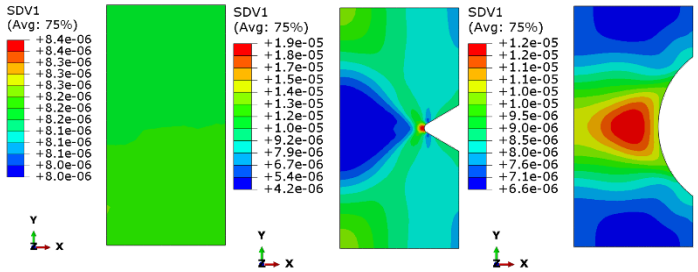

FIGURE 13: THE CONTOURS OF THE INELASTIC STRAIN RATE AT THE INITIAL 10 S HOLD OF THE 3RD CYCLE OF UNIFORM AND NOTCH SPECIMENS

In an attempt to quantitatively investigate the geometric effect on elastic follow-up factor and study the effect of elastic follow-up on relaxation behavior, in this study, the elastic follow-up factors were also calculated using the numerical results. A schematic of the stress strain curve of tensile-hold CF test illustrating definition of elastic follow-up factor and the mixed stress-strain-controlled mode is presented in Figure 14. The elastic follow-up factor, q, is generally defined as a ratio of increased inelastic/creep strain $\Delta\epsilon_{in}$ and the elastic strain $\Delta\epsilon_e$ during hold-time period under the uniaxial loading condition, given by Eq. 24:

$$q = -\frac{\Delta\epsilon_{in}}{\Delta\epsilon_e} \tag{24}$$

Compared with the strain-controlled mode (i.e., elastic follow-up factor $q = 1$) for the uniaxial uniform specimens, discontinuous geometric shapes of notch specimens always induce the mixed stress-strain-controlled mode. In this case, the elastic follow-up phenomenon contributes to the decrease of stress relaxation rate during hold time and hence the enhanced creep damage to the component. In the multiaxial stress state, the elastic follow-up factor can be calculated using Eq. 25 [9]:

$$q = -\frac{\Delta W_{in}}{\Delta W_e} \tag{25}$$

where ΔW_{in} is the changes in inelastic strain energy and ΔW_e is changes in elastic strain energy at holding period. Moreover, the magnitude of time interval in Eq. 25 reveals a difference between a tangent and a secant definition of the elastic follow-up for a structural component. In the current study, the elastic follow-up factor was calculated in each element based on Eq. 25. The near-tangent values of elastic follow-up are calculated using data of the initial 10 s during the holding.

Figure 15 shows the contours of elastic follow-up factor of shallow-notch and V-notch specimens. An elastic follow-up factor of about 1.5, in general is induced by two notch geometries.

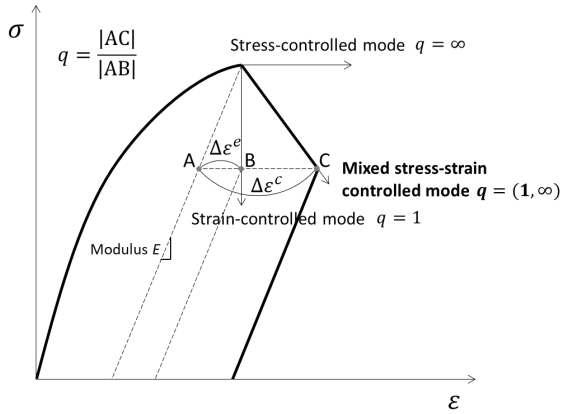

FIGURE 14: SCHEMATIC OF THE DEFINITION OF ELASTIC FOLLOW-UP FACTOR.

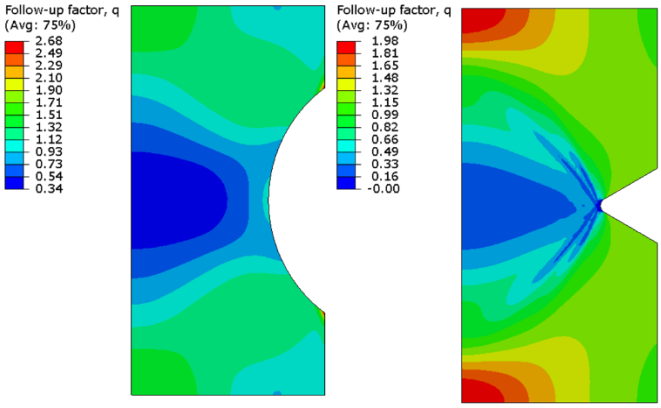

FIGURE 15: THE CONTOURS OF THE ELASTIC FOLLOW-UP FACTOR Q OF SHALLOW-NOTCH AND V-NOTCH SPECIMENS.

As described above, notch geometry causes the multiaxial stress state and elastic follow-up phenomenon, which, as expected in turn, would influence the relaxation behavior during the hold period. To qualitatively illustrate the multi-axial stress state and elastic follow-up effects on stress relaxation behavior, Figure 16 shows the normalized stress relaxation curves with given stress triaxiality factor and elastic follow-up factor collected from FE results. Note that the case of TF=0.333 and q=1.0 represents the uniform specimen under uniaxial loading condition. As shown in Figure 16, it is likely that both triaxiality factor and follow-up factor plays roles in the increase of stress relaxation rate.

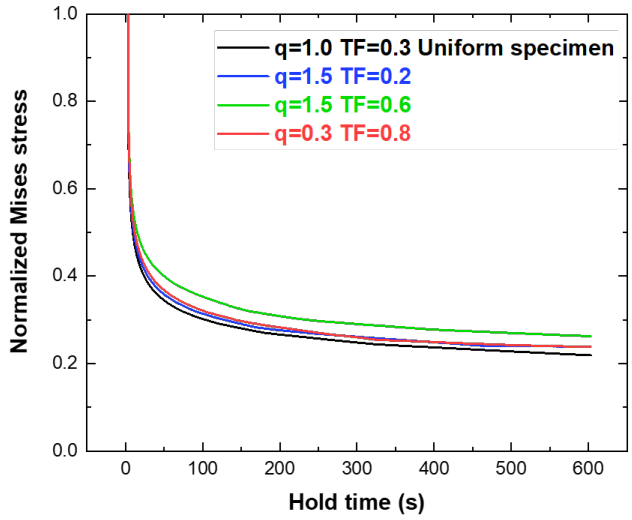

FIGURE 16: EXAMPLES OF THE NORMALIZED STRESS RELAXATION CURVES AT THE 3RD CYCLE WITH DIFFERENT GIVEN STRESS TRIAXIALITY FACTOR AND ELASTIC FOLLOW-UP FACTOR.

Finally, the experimental data associated with numerical equivalent strain range of shallow-notch specimens with tensile hold times of 600 s and 3600 s are plotted in Figure 17. Here we did not add the data of V-notch specimen since the cycle to failure is hard to be determined by using the current experimental data.

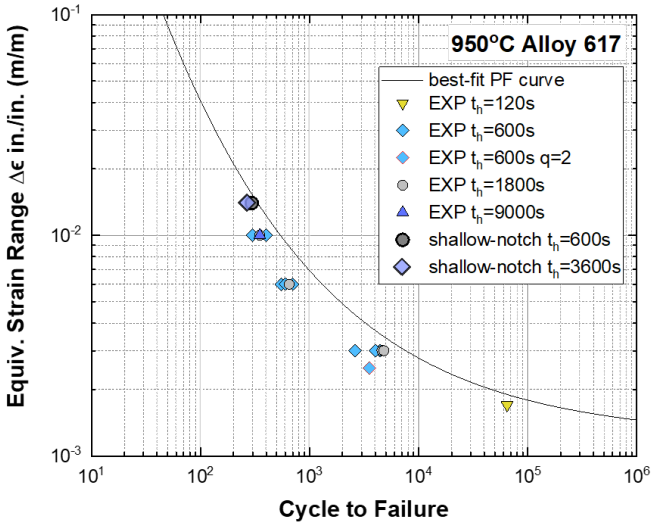

FIGURE 17: TENSILE-HOLD CREEP-FATIGUE (CF) EXPERIMENTAL DATA FOR ALLOY 617 AT 950°C ALONG WITH CF DATA OF NOTCH SPECIMENS.

5. CONCLUSION

Two types of notch specimen geometries, shallow-notch and sharp V-notch were designed for Alloy 617 per ASTM Standard E292-09. The experimental creep-fatigue (CF) tests on notch specimens were conducted at temperature of 950°C to investigate the role of notch geometry on the stress relaxation behavior and CF life. The experimental results of notch specimens were compared to the standard CF experimental data of uniform specimens. In addition, a unified viscoplasticity model was implemented into finite element simulation through a user defined material subroutine in ABAQUS. Numerical simulation was conducted to incorporate to experimental results and to investigate the multi-axial stress relaxation and the role of elastic follow-up effect on the effectiveness of notch geometry in resisting the stress relaxation. Main observations and conclusions are as follows:

The CF life is reduced in notch specimens in comparison to uniform specimens at same uniaxial testing condition. The effect of tensile hold time on the CF life in notch specimens is not significant. Comparing to uniform specimens, notch specimens exhibit higher relaxation stresses, but having a comparable stress relaxation rate.

Through numerical simulations on two types of notch geometry, it is likely that the stress triaxiality factor and elastic follow-up factor have the responsibilities for the reduction in stress relaxation rate. Also, it seems being sensible to use equivalent strain range to display the CF data of notch specimens on the strain range-cycle curve.

COPYRIGHT NOTICE

ACKNOWLEDGMENTS

The research was sponsored by the U.S. Department of Energy, Office of Nuclear Energy, under contract No. DE-AC05-00OR22725 with Oak Ridge National Laboratory (ORNL), managed and operated by UT-Battelle, LLC, and under contract No. DE-AC07-05ID14517 with Idaho National Laboratory (INL), managed and operated by Battelle Energy Alliance, LLC. Programmatic direction was provided by the Office of Nuclear Reactor Deployment of the Office of Nuclear Energy.

The contribution of Charles S. Hawkins and Brad Hall of ORNL in running the experiments is greatly appreciated.

REFERENCES

[1] Wang, Y., Jetter, R. I., and Sham, T.-L. (2016a), "FY16 Progress Report on Test Results In Support Of Integrated EPP and SMT Design Methods Development" ORNL/TM-2016/330, Oak Ridge National Laboratory, Oak Ridge, Tennessee.

[2] Wang, Y., Jetter, R. I., and Sham, T.-L. (2016b), "Preliminary Test Results in Support of Integrated EPP and SMT Design Methods Development," ORNL/TM-2016/76, Oak Ridge National Laboratory, Oak Ridge, Tennessee.

[3] Wang, Y., Jetter, R.I., and Sham, T.-L. (2017a), "Report on FY17 Testing in Support of Integrated EPP-SMT Design Methods Development," ORNL/TM-2017/351, Oak Ridge National Laboratory, Oak Ridge, Tennessee.

[4] ASTM E292-09, 2009. Standard test method for conducting time-for-rupture notch tension tests of materials. ASTM International, West Conshohocken, Pennsylvania.

[5] ASMT E2714, "Standard Test Method for Creep-Fatigue Testing," ASTM International, West Conshohocken, Pennsylvania

[6] Wright, R.N. (2021), "Draft ASME Boiler and Pressure Vessel Code Cases and Technical Bases for Use of Alloy 617 for Construction of Nuclear Components Under Section Ill, Division 5," INL/EXT-15-36305 Revision 2, Idaho National Laboratory, Idaho Falls, Idaho.

[7] Messner, M.C. (2022). ASME Code Revisions to Incorporate 316H and Alloy 617 Viscoplastic Constitutive Models to Section III, Division 5 and Code Case N-898 (No. ANL-ART-249). Argonne National Lab.(ANL), Argonne, IL (United States).

[8] Messner, M.C. and Sham, T.L. (2021). A Viscoplastic Model for Alloy 617 for Use With the ASME Section III, Division 5 Design by Inelastic Analysis Rules. In Pressure Vessels and Piping Conference (Vol. 85314, p. V001T01A034). American Society of Mechanical Engineers.

[9] Messner, M. C., Jetter. B, and Sham, T. L. (2019), "A Method for Directly Assessing Elastic Follow Up in 3D Finite Element Calculations," Proceedings of the ASME 2019 Pressure Vessels & Piping Conference, PVP2019-93644, American Society of Mechanical Engineers, New York.